

## Higher-order moments of the elliptic flow distribution in lead-lead collisions at $\sqrt{s_{\text{NN}}} = 5.02$ TeV

---

**Jovan Milosevic on behalf of the CMS Collaboration\***

*Department of physics, "VINČA" Institute of Nuclear Science - National Institute of the Republic of Serbia, Mike Petrovica Alasa 12-14, University of Belgrade, Belgrade, Serbia*

*E-mail: [jmilos@vin.bg.ac.rs](mailto:jmilos@vin.bg.ac.rs)*

The collective anisotropic hydrodynamic behavior of charge hadrons is studied using the multiparticle correlation method. The elliptic anisotropy harmonic from different orders of multiparticle cumulants,  $v_2\{2k\}$ , are measured up to the tenth order ( $k = 5$ ) as functions of the collision centrality in lead-lead collisions at an energy of  $\sqrt{s_{\text{NN}}} = 5.02$  TeV. The data were collected by the CMS experiment at the LHC, with an integrated luminosity of  $0.58 \text{ nb}^{-1}$ . A fine splitting  $v_2\{2\} > v_2\{4\} \gtrsim v_2\{6\} \gtrsim v_2\{8\} \gtrsim v_2\{10\}$  is observed. The subtle differences in the higher-order cumulants allow for a precise determination of the underlying hydrodynamics. Based on these results, centrality-dependent moments for the fluctuation-driven event-by-event  $v_2$  distribution are determined, including the skewness, the kurtosis and, for the first time, the superskewness. Assuming a hydrodynamic expansion of the produced medium, these moments probe the initial-state geometry in high-energy nucleus-nucleus collisions.

*11th International Conference of the Balkan Physical Union (BPU11),  
28 August - 1 September 2022  
Belgrade, Serbia*

---

\*Speaker

## 1. Introduction

A hot and dense state of strongly interacting quarks and gluons, the so-called quark-gluon plasma (QGP), is created in nucleus-nucleus collisions at high-energies. The evidence for this state was first obtained at the BNL RHIC [1–4]. Experiments at the CERN LHC, performed with nucleus-nucleus collisions at much higher energies, confirmed the RHIC results with much larger event samples and kinematic ranges. An important feature of the QGP is its collective, hydrodynamic expansion. The initial spatial geometry of the overlap region of the colliding nuclear densities results in anisotropic pressure gradients that, in turn, are reflected in the azimuthal anisotropic distribution of emitted particles. This anisotropy is used to perform detailed studies of the QGP formed at the LHC [5–17]. Fluctuations in the position of nucleons in the incident nuclei have a significant influence on the QGP expansion [6, 10, 18–20]. The study of the event-by-event fluctuations can give insight into the early stage dynamics of the collisions [21–23].

The elliptic flow harmonic  $v_2$  is the leading term of a Fourier series expansion of the azimuthal angle distributions in the event plane frame (defined by the beam direction and the direction of maximum emitted particle density) [24, 25]. The cumulant method, introduced in Refs. [26, 27], is based on multiparticle correlations in the laboratory frame. Cumulants obtained by correlating four or more particles are able to suppress short-range correlations arising from jets and resonance decays. The  $v_2$  value can be determined by measuring correlations among the emitted particles. This involves relating the  $v_2$  values to cumulants  $c_2\{2k\}$ , where  $2k$  is the cumulant order. A direct correlation exists between  $v_n\{2k\}$  and  $c_n\{2k\}$  values, where  $n$  is the order of the Fourier harmonic. For example,  $v_2\{2\}$ ,  $v_2\{4\}$ , and  $v_2\{6\}$  are referred to as the 2-, 4-, and 6-particle cumulant based values for the  $v_2$ , respectively. In this analysis, the  $v_2\{2k\}$  values are determined using the Q-cumulant method in which one calculates multi-particle cumulants in terms of moments of Q-vectors [28]. Fluctuation behavior can be studied based on the  $v_2\{2k\}$  ( $k = 1, 2, 3, \dots$ ) values [27]. For Gaussian fluctuations, the  $v_2\{2k\}$  values with  $k > 1$  are all expected to have the same value [29]. However, the measured higher-order  $v_2\{2k\}$  ( $k = 2, 3, 4$ ) show a fine splitting [30, 31] that is a consequence of the non-Gaussian behavior of the fluctuations [32]. In Ref. [33] it is noted that the main signature of non-Gaussian fluctuations is a nonzero skewness of the  $v_2$  distribution. This suggests, as described in Ref. [33], a hydrodynamic probe defined by the ratio  $(v_2\{6\} - v_2\{8\}) / (v_2\{4\} - v_2\{6\})$ . The basic premise of a hydrodynamic probe is that the observed azimuthal correlations of the bulk medium can be directly related to the initial-state geometry.

This analysis has been performed with measurement of the ten-particle cumulant based  $v_2\{10\}$  values for lead-lead (PbPb) collisions at  $\sqrt{s_{NN}} = 5.02$  TeV, collected by the CMS experiment at the LHC, with an integrated luminosity of  $0.58 \text{ nb}^{-1}$  [34]. This enables us to develop a new hydrodynamic probe using the  $v_2\{10\}$  value and the corresponding values for lower-order cumulant based  $v_2\{2k\}$ . The new hydrodynamic probe is defined as the ratio  $(v_2\{8\} - v_2\{10\}) / (v_2\{6\} - v_2\{8\})$ . These two hydrodynamic probes should be independent of centrality if higher-order moments of the  $v_2$  distribution are negligible. The centrality is expressed as a percentile of the total inelastic hadronic cross section. The events with 0% centrality have the largest overlap of the two colliding nuclei. The experimental evidence for a significant centrality dependence, presented in this contribution, indicates that higher-order moments are not negligible.

The powers in the expansion of the elliptic flow generating function into a Taylor series

correspond to the higher-order central moments of the  $v_2$  distribution. The skewness ( $s$ ) is the 3<sup>rd</sup> central moment and describes the asymmetry of the  $v_2$  distribution. The kurtosis ( $\kappa$ ) is the 4<sup>th</sup> central moment and describes peakedness of the center and heaviness of the tail of the distribution. The superskewness ( $p$ ) is the 5<sup>th</sup> central moment and gives a measure of the relative importance of the tails as compared to the central part of the distribution. In this analysis, a second hydrodynamic probe is introduced that uses the  $v_2\{10\}$  value. It is shown that both the original and the new probe require the inclusion of higher-order central moments to describe their observed centrality dependence. The kurtosis is needed for the original probe, and both the kurtosis and the superskewness for the second. Precise measurements of the fluctuation-driven moments of the  $v_2$  distribution place stringent constraints on hydrodynamic predictions of the QGP evolution.

## 2. The CMS detector and data used

The central feature of the CMS apparatus is a superconducting solenoid of 6 m internal diameter, providing a magnetic field of 3.8 T. Within the solenoid volume are a silicon pixel and strip tracker, a lead tungstate crystal electromagnetic calorimeter, and a brass and scintillator hadron calorimeter, each composed of a barrel and two endcap sections. Forward calorimeters (HF), made of steel and quartz-fibres, extend the pseudorapidity coverage provided by the barrel and endcap detectors. Muons are measured in gas-ionization detectors embedded in the steel flux-return yoke outside the solenoid. Events of interest are selected using a two-tiered trigger system. The first level (L1), composed of custom hardware processors, uses information from the calorimeters and muon detectors to select events at a rate of around 100 kHz [35]. The second level, known as the high-level trigger (HLT), consists of a farm of processors running a version of the full event reconstruction software optimized for fast processing, and reduces the event rate to around 1 kHz before data storage [36]. A more detailed description of the CMS detector, together with a definition of the coordinate system used and the relevant kinematic variables, can be found in Ref. [37].

The data analyzed in this contribution, before applying the selection described below, consist of  $4.27 \cdot 10^9$  minimum bias lead-lead (PbPb) collisions at  $\sqrt{s_{NN}} = 5.02$  TeV, collected in 2018 with an integrated luminosity of  $0.58 \text{ nb}^{-1}$  [38]. The minimum bias events are triggered by requiring signals above readout thresholds of 3 GeV in each of the two HF calorimeters [36]. The events are required to have at least one reconstructed primary vertex (based on two or more tracks) within a distance ( $|z_{\text{vtx}}|$ ) of 15 cm from the nominal interaction point along the beam axis. The primary vertex is selected as the one with the highest track multiplicity in the event.

More technical details about tracks selection and their efficiency corrections can be found in Ref. [34]. In this analysis, the systematic uncertainties are determined by varying the vertex selection, the track selection, the centrality determination, and the efficiency correction. The detailed description about these sources of the systematic uncertainties can be found in Ref. [34].

## 3. Analysis procedure

An improved version of the cumulant method, the Q-cumulant method, introduced in Ref. [28], is based on the flow vector  $Q_n = \sum_{j=1}^M e^{in\phi_j}$ . Here,  $n$  is the flow harmonic order,  $M$  denotes the

event multiplicity, i.e., the number of analyzed tracks in the given event, and  $\phi_j$  is the laboratory azimuthal angle of the track indexed with  $j$ . The relations between the flow vector  $Q_n$  and  $2m$ -particle azimuthal correlators  $\langle 2m \rangle$  as well as its weighted mean  $\langle\langle 2m \rangle\rangle$  are defined in Ref. [28]. The  $2m$  represents the cumulant order. The double brackets  $\langle\langle \dots \rangle\rangle$  denote a weighted average over all events within a given centrality class. From the recursion relationship for the  $c_n\{2k\}$  values given in Ref. [39], the  $c_n\{10\}$  value is determined as

$$c_n\{10\} = \langle\langle 10 \rangle\rangle - 25\langle\langle 2 \rangle\rangle\langle\langle 8 \rangle\rangle - 100\langle\langle 4 \rangle\rangle\langle\langle 6 \rangle\rangle + 400\langle\langle 6 \rangle\rangle\langle\langle 2 \rangle\rangle^2 + 900\langle\langle 2 \rangle\rangle\langle\langle 4 \rangle\rangle^2 - 3600\langle\langle 4 \rangle\rangle\langle\langle 2 \rangle\rangle^3 + 2880\langle\langle 2 \rangle\rangle^5. \quad (1)$$

From a general formula that relates the  $v_n\{2k\}$  and the  $c_n\{2k\}$  values, given in Ref. [34], the formula for the  $v_n\{10\}$  is given as

$$v_n\{10\} = \sqrt[10]{\frac{1}{456}c_n\{10\}}. \quad (2)$$

#### 4. Hydrodynamic probes

The cumulant expansion formulation is given through the formalism of generating functions. The Fourier–Laplace transform of the symmetry plane elliptic harmonic vector  $\mathbf{v}_2 = v_x\mathbf{e}_x + v_y\mathbf{e}_y$  is  $\langle e^{\mathbf{l}\cdot\mathbf{v}_2} \rangle$ , where the brackets indicate the average of events within a centrality class. Here,  $\mathbf{l} = l_x\mathbf{e}_x + l_y\mathbf{e}_y$  is a vector variable with  $\mathbf{e}_x$  denoting the unit vector in the symmetry plane perpendicular to the beam axis, while  $\mathbf{e}_y$  is the unit vector perpendicular to the symmetry plane. The symmetry plane is defined in terms of the beam direction and the impact parameter vector  $\mathbf{b}$ . The vector  $\mathbf{b}$  connects imagined centers of the colliding nuclei in the perpendicular to the beam axis. The experimentally accessible event plane is, on average, in the same direction as the symmetry plane, but fluctuates around it because of resolution effects due to finite particle multiplicities. In Ref. [33], the generating function of the cumulants is defined as  $\ln\langle e^{\mathbf{l}\cdot\mathbf{v}_2} \rangle$ . If one expands this generating function up to the 4<sup>th</sup> power in  $(l_x, l_y)$  one gets the expression in terms of central moments of the  $(v_x, v_y)$  distribution, that includes the variance ( $\sigma$ ),  $s$ , and  $\kappa$  [40]. By extending this expansion up to the 5<sup>th</sup> power in  $(l_x, l_y)$ , in Ref. [34] is obtained the expression that contains additional terms that include  $p$  central moments of the  $(v_x, v_y)$  distribution:

$$\begin{aligned} \ln\langle e^{\mathbf{l}\cdot\mathbf{v}_2} \rangle \approx & l_x\bar{v}_2 + \frac{1}{2!}(l_x^2\sigma_x^2 + l_y^2\sigma_y^2) + \frac{1}{3!}(l_x^3s_{30} + 3l_xl_y^2s_{12}) + \frac{1}{4!}(l_x^4\kappa_{40} + 6l_x^2l_y^2\kappa_{22} + l_y^4\kappa_{04}) \\ & + \frac{1}{5!}(l_x^5p_{50} + 10l_x^3l_y^2p_{32} + 5l_xl_y^4p_{14}). \end{aligned} \quad (3)$$

The higher-order central moments are defined as in Refs. [34, 40].

By following the procedure for expanding the generating function of the  $v_2\{2k\}$ , as described in Ref. [33], one can express them in terms of the central moments. In difference to the derivation performed in [33], the current analysis additionally covers the 4<sup>th</sup> and 5<sup>th</sup> moments. The corresponding formulas for the  $v_2\{2k\}$  can be found in [34].

If one neglects the 5<sup>th</sup>-order moments  $p$ , as well as the terms with the multiplier  $(\sigma_y^2 - \sigma_x^2)$ , then the first hydrodynamic probe given in Ref. [33] can be expressed as

$$\frac{v_2\{6\} - v_2\{8\}}{v_2\{4\} - v_2\{6\}} \approx \frac{1}{11} - \frac{4\kappa_{40}}{11[2\bar{v}_2 s_{30} + 3(\kappa_{40} + \kappa_{22})]}. \quad (4)$$

Neglecting the kurtosis  $\kappa$  moment would reduce the right-hand side of Eq. (4) to a constant value of 1/11. To check the approximation given by Eq. (4) experimentally, one would need to express its right-hand side through the measurable quantities  $v_2\{2k\}$  [34].

$$h_1 = \frac{v_2\{6\} - v_2\{8\}}{v_2\{4\} - v_2\{6\}} \approx h_1^{\text{Taylor}} = \frac{1}{11} - \frac{1}{11} \frac{v_2\{4\}^2 - 12v_2\{6\}^2 + 11v_2\{8\}^2}{v_2\{4\}^2 - v_2\{6\}^2}. \quad (5)$$

In the above relation,  $h_1$  denotes the hydrodynamic probe and  $h_1^{\text{Taylor}}$  denotes the corresponding Taylor expansion of this probe expressed through the  $v_2\{2k\}$  values.

By employing the  $v_2\{10\}$  harmonic, the hydrodynamic probe  $h_2$ , expressed in terms of the moments in the expansion of the  $v_2$  generating function, is given by

$$\begin{aligned} & \frac{v_2\{8\} - v_2\{10\}}{v_2\{6\} - v_2\{8\}} \approx \\ & \approx \frac{3}{19} + \frac{88p_{50}}{95[4s_{30}\bar{v}_2^2 - 2\bar{v}_2(\kappa_{40} - 3\kappa_{22}) - (13p_{50} + 10p_{32} - 3p_{14}) - 2(\sigma_y^2 - \sigma_x^2)(5s_{30} - 6s_{12})]}. \end{aligned} \quad (6)$$

Similarly to the  $h_1$ , the new hydrodynamic probe,  $h_2$ , can be Taylor expanded and expressed in terms of the measured  $v_2\{2k\}$  values as

$$h_2 = \frac{v_2\{8\} - v_2\{10\}}{v_2\{6\} - v_2\{8\}} \approx h_2^{\text{Taylor}} = \frac{3}{19} - \frac{1}{19} \frac{3v_2\{6\}^2 - 22v_2\{8\}^2 + 19v_2\{10\}^2}{v_2\{6\}^2 - v_2\{8\}^2}. \quad (7)$$

## 5. The standardized and corrected moments

The standardized skewness,  $\gamma_1^{\text{exp}}$ , and kurtosis,  $\gamma_2^{\text{exp}}$ , expressed in terms of the  $v_2\{2k\}$  values, are given by Eq. (15) in Ref. [40]. The standardized superskewness,  $\gamma_3$ , is defined as

$$\gamma_3 \equiv \frac{p_{50}}{\sigma_x^5}. \quad (8)$$

In order to express the standardized superskewness through the measured  $v_2\{2k\}$  values with  $k = 1, \dots, 5$ , one can use the expansion of the fifth power of the  $v_2\{2k\}$  value. The expression for the experimentally measured superskewness is then given as

$$\gamma_3^{\text{exp}} = 6\sqrt{2} \frac{3v_2\{6\}^5 - 22v_2\{8\}^5 + 19v_2\{10\}^5}{(v_2\{2\}^2 - v_2\{4\}^2)^{5/2}}. \quad (9)$$

The standardized moments,  $\gamma_i^{\text{exp}}$  ( $i = 1, 2, 3$ ), have contributions from higher-order moments of the  $v_2$  distribution that are not negligible (more details in Ref. [34]). As it has been shown in

Ref. [34], the “corrected” (“cleaned”) moments, which are free of contributions from higher-order moments, can be also expressed through measurable  $v_2\{2k\}$  values. As an example, the corrected skewness can be expressed as

$$\gamma_{1,\text{corr}}^{\text{exp}} = -2^{3/2} \frac{187v_2\{8\}^3 - 16v_2\{6\}^3 - 171v_2\{10\}^3}{(v_2\{2\}^2 - 40v_2\{6\}^2 + 495v_2\{8\}^2 - 456v_2\{10\}^2)^{3/2}}. \quad (10)$$

The same correction procedure, as described in Ref. [34], can also be applied to the standardized kurtosis and the standardized superskewness. The corrected form of these moments are then determined as

$$\gamma_{2,\text{corr}}^{\text{exp}} = -\frac{3}{2} \frac{v_2\{4\}^4 + 24v_2\{6\}^4 - 253v_2\{8\}^4 + 228v_2\{10\}^4}{(v_2\{2\}^2 - 40v_2\{6\}^2 + 495v_2\{8\}^2 - 456v_2\{10\}^2)^2}, \text{ and} \quad (11)$$

$$\gamma_{3,\text{corr}}^{\text{exp}} = 6\sqrt{2} \frac{3v_2\{6\}^5 - 22v_2\{8\}^5 + 19v_2\{10\}^5}{(v_2\{2\}^2 - 40v_2\{6\}^2 + 495v_2\{8\}^2 - 456v_2\{10\}^2)^{5/2}}. \quad (12)$$

## 6. Results

It was previously shown in Ref. [33] that the presence of non-Gaussian fluctuations in the initial-state energy density leads to a fine splitting between the higher-order  $v_2\{2k\}$  values. The  $v_2\{2k\}$  ( $k = 1, \dots, 5$ ) values are presented in Fig. 1 as functions of centrality in PbPb collisions at  $\sqrt{s_{\text{NN}}} = 5.02$  TeV. The results are obtained from charged particles detected within  $|\eta| < 2.4$ , and with  $0.5 < p_T < 3.0$  GeVc. The systematic uncertainties are about 2 orders of magnitude greater than the statistical ones. A clear splitting between the  $v_2\{2\}$  and higher-orders cumulant based  $v_2\{2k\}$  ( $k = 2, \dots, 5$ ) values is visible, with  $v_2\{2\}^2 \approx v_2\{2k\}^2 + 2\sigma_v^2$  for  $k > 1$  and where  $\sigma_v^2$  is the  $v_2$  variance related to flow fluctuations [33]. From Fig. 1 it is clear that the flow fluctuations become larger going to more peripheral collisions.

The measured  $v_2\{2k\}$  ( $k = 1, \dots, 5$ ) values are used to calculate the hydrodynamic probes given by the left-hand sides of Eqs. (5) and (7). Figure 2 displays these distributions with closed symbols, while with open symbols are shown the right-hand sides of Eqs. (5) and (7). The last are also constructed using the measured  $v_2\{2k\}$  ( $k = 1, \dots, 5$ ) values.

As a consequence of the low multiplicities involved in the calculation of the  $v_2\{2k\}$ , statistical uncertainties quickly increase as peripheral collisions are approached. For very central collisions, because of the small  $v_2\{2k\}$  magnitudes, the relative statistical uncertainties are larger and thus statistical uncertainties of the hydrodynamic probes are increased. The magnitudes of the statistical uncertainties of the  $h_2$  distribution are larger with respect to those corresponding to the  $h_1$  distribution because higher-order cumulants are involved. The distributions themselves show a weak centrality dependence. With an exception of the first analyzed bin, they have their lowest magnitudes around 10–20% centrality range, and the magnitude show a trend of a slow increase going to peripheral collisions. Based on an event-by-event measurement of the  $v_2$  distribution, it was reported in Ref. [30] that the  $h_1$  has a value of  $0.143 \pm 0.008$  (stat)  $\pm 0.014$  (syst) for 20–25%

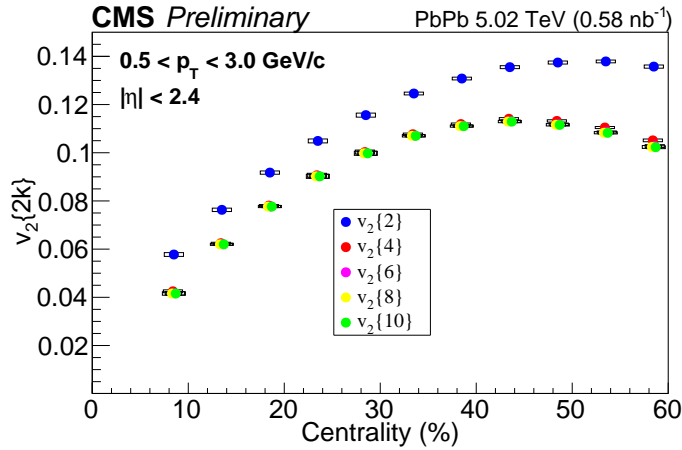


**Figure 1:** The  $v_2\{2k\}$  ( $k = 1, \dots, 5$ ) values as functions of centrality in PbPb collisions at  $\sqrt{s_{NN}} = 5.02$  TeV. The measurement is performed with charged particles within the acceptance region. The vertical sizes of the open boxes denote the systematic uncertainties. Statistical uncertainties are negligible compared to the marker size. The centrality value is the center of the interval without uncertainty. The figure is taken from Ref. [34].

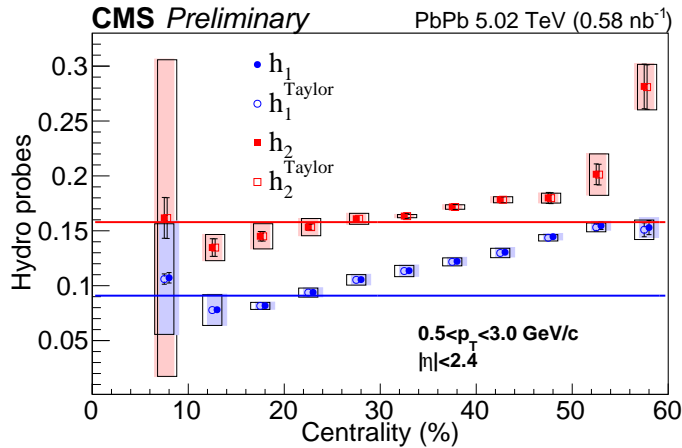


**Figure 2:** The  $h_1$  (closed blue circles) and the  $h_2$  (closed red squares) hydrodynamic probes as functions of centrality in PbPb collisions at  $\sqrt{s_{NN}} = 5.02$  TeV. The distributions depicted with the open circles and squares represent the corresponding Taylor expansions given by  $h_1^{\text{Taylor}}$  and  $h_2^{\text{Taylor}}$ , respectively. The horizontal blue (red) line represents a constant value of  $1/11$  ( $3/19$ ). The measurement is performed with charged particles within the acceptance region. The bars (the vertical sizes of the open boxes) denote the statistical (systematic) uncertainties. The centrality value is the center of the interval without uncertainty. The figure is taken from Ref. [34].

central events, and increases to  $0.185 \pm 0.005$  (stat)  $\pm 0.012$  (syst) as the centrality increases to 55–60%. Using the Q-cumulant method, Ref. [31] compares the measured  $v_2\{6\} - v_2\{8\}$  and  $\frac{1}{11}(v_2\{4\} - v_2\{6\})$  distributions. One should take into account the differences in the acceptances between the current and these previous analyses. [30, 31]. Although with larger uncertainties, these results are qualitatively similar to the results from the current analysis. There is a very good

agreement between the distributions obtained by the expressions given on left-hand and right-hand sides of Eq. (5) and Eq. (7) in Fig. 2. This indicates the importance of including higher-order terms in the Taylor expansion of the  $v_2$  generating function.

Figure 3 displays the distributions of the measured skewness  $\gamma_1^{\text{exp}}$ , kurtosis  $\gamma_2^{\text{exp}}$ , and the superskewness  $\gamma_3^{\text{exp}}$  as functions of centrality. The distributions of the corrected skewness  $\gamma_{1,\text{corr}}^{\text{exp}}$  (upper), kurtosis  $\gamma_{2,\text{corr}}^{\text{exp}}$  (middle), and superskewness  $\gamma_{3,\text{corr}}^{\text{exp}}$  (lower) are presented with the open blue circles. The systematic uncertainties are generally larger than the statistical ones.

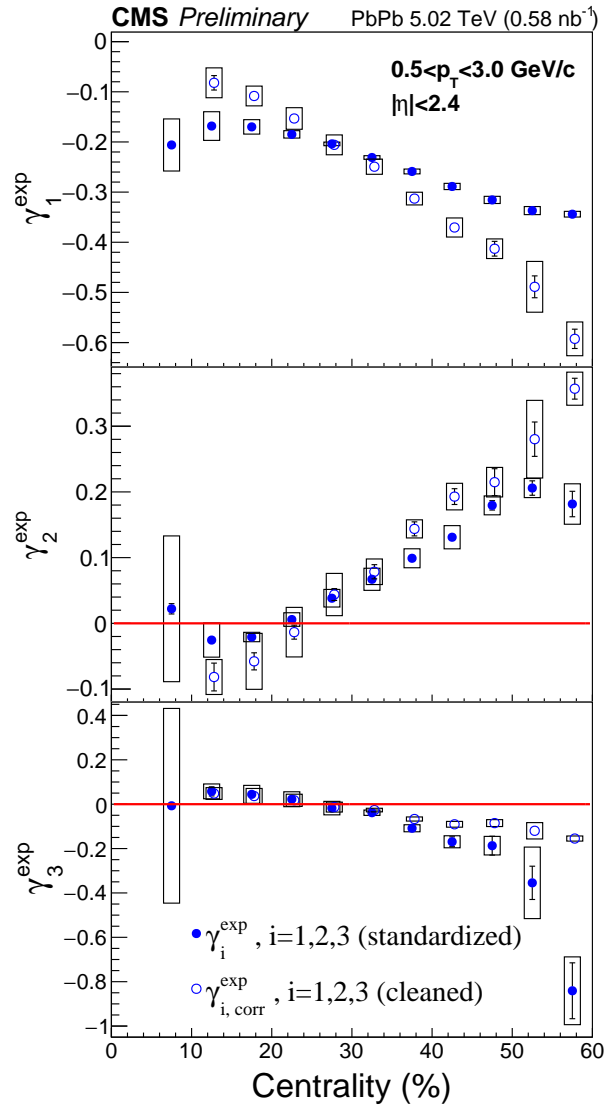


**Figure 3:** The magnitudes of the measured (closed circles) skewness  $\gamma_1^{\text{exp}}$  (upper), kurtosis  $\gamma_2^{\text{exp}}$  (middle), and the superskewness  $\gamma_3^{\text{exp}}$  (lower) as functions of centrality in PbPb collisions at  $\sqrt{s_{\text{NN}}} = 5.02$  TeV. The magnitudes of the “corrected” skewness  $\gamma_{1,\text{corr}}^{\text{exp}}$  (upper), kurtosis  $\gamma_{2,\text{corr}}^{\text{exp}}$  (middle), and superskewness  $\gamma_{3,\text{corr}}^{\text{exp}}$  (lower) are presented with the open circles. The measurement is performed with charged particles within the acceptance region. The bars (the vertical sizes of the open boxes) denote statistical (systematic) uncertainties. The centrality value is the center of the interval without uncertainty. The figure is taken from Ref. [34].

The  $\gamma_1^{\text{exp}}$  is negative over the entire analyzed centrality range. This is a consequence of the  $v_{2,x}$  distribution having a long tail on the low  $v_{2,x}$  side (as shown in Fig.1 of Ref. [33]). The  $v_{2,y}$  distribution is symmetric and thus its skewness is equal to zero. The  $\gamma_1^{\text{exp}}$  has been predicted to become more negative as the centrality percentile increases [33]. This measurement confirms the prediction. The  $\gamma_2^{\text{exp}}$  values are positive over nearly the entire analyzed centrality range. The exception is cross out for the centrality range of 10–20%. The sign of  $\gamma_2^{\text{exp}}$  is driven by the mean eccentricity  $\epsilon_0$ , and is negative for  $\epsilon_0 < 0.28$  and positive for  $\epsilon_0 > 0.29$  [40]. Our results are qualitatively in an agreement with this prediction. If the  $v_2$  values were a pure linear response to the initial-state eccentricity  $\epsilon_2$ , the corresponding kurtosis will be equal to the kurtosis of the initial  $\epsilon_2$  fluctuations. Although a fully linear response is not expected, calculations predict that the non-Gaussianities (skewness and kurtosis), although significantly reduced by the hydrodynamic evolution, are still influenced by the early stage hydrodynamics [33]. Except for collisions with centralities less than 25%, where it is either positive or vanishes, the  $\gamma_3^{\text{exp}}$  moment is negative with its absolute magnitude increasing towards more peripheral collisions. This is the first measurement of this moment of the  $v_2$  distribution. Without the superskewness it would be impossible to describe the centrality dependence observed for the new hydrodynamic probe  $h_2$ .

In addition to the experimental results for the standardized skewness, kurtosis, and superskewness, the corresponding cleaned, i.e. the corrected moments are also presented. Except for the superskewness, the corrected skewness and kurtosis have larger slopes with respect to the standardized ones. The corrected moments give additional constraints on models of the initial-state geometry.

## 7. Summary

The cumulants of the elliptic flow distribution  $v_2\{2k\}$  ( $1 \leq k \leq 5$ ) are determined as functions of centrality in lead-lead (PbPb) collisions at  $\sqrt{s_{\text{NN}}} = 5.02$  TeV, with an integrated luminosity of  $0.58 \text{ nb}^{-1}$ . For the first time, the  $v_2\{10\}$  value is determined. A fine splitting is observed between the cumulants, with  $v_2\{4\} \gtrsim v_2\{6\} \gtrsim v_2\{8\} \gtrsim v_2\{10\}$ . This splitting is attributed to a non-Gaussian behavior in the event-by-event fluctuations of the  $v_2$  distribution leading to nonzero values of the skewness, kurtosis, and the superskewness of this distribution. The splitting becomes finer as the  $k$  value increases, and the difference between the adjacent  $v_2\{2k\}$  decrease by about an order of magnitude. The standardized magnitude of the  $v_2$  moments are presented, together with their corrected values, where contributions from higher-order moments (up to the 5<sup>th</sup> moment) are removed. The hydrodynamic probes are measured as a function of centrality, with values slowly increasing going to more peripheral collisions. This contrasts with an earlier hydrodynamic expectation that had taken the skewness of the initial-state geometry as the main source of non-Gaussian fluctuations. In this case, the probes are not expected to depend on centrality. The observed centrality dependences can be understood in terms of the evolving shape of the interaction region with centrality. This is shown by performing a Taylor expansion of the  $v_2$  cumulant generating function up to the 4<sup>th</sup> (5<sup>th</sup>) moment, as expressed in terms of the measured  $v_2\{2k\}$ , for the first (second) hydrodynamic probe. Theoreticians can tune hydrodynamics models such to reconstruct our measured moments. Thus, these results place further constraints on the initial-state geometry

which could be useful in future hydrodynamic calculations of the medium expansion in high-energy nucleus-nucleus collisions.

## Acknowledgments

The authors acknowledge the support from Ministry of Education Science and Technological Development, Republic of Serbia.

## References

- [1] I. Arsene et al., BRAHMS Collaboration, Nucl. Phys. A **757** (2005) 1
- [2] B. B. Back et al., PHOBOS Collaboration, Nucl. Phys. A **757** (2005) 28
- [3] J. Adams et al., STAR Collaboration, Nucl. Phys. A **757** (2005) 102
- [4] K. Adcox et al., PHENIX Collaboration, Nucl. Phys. A **757** (2005) 184
- [5] K. Aamodt et al., ALICE Collaboration, Phys. Rev. Lett. **105** (2010) 252302
- [6] K. Aamodt et al., ALICE Collaboration, Phys. Rev. Lett. **107** (2011) 032301
- [7] B. B. Abelev et al., ALICE Collaboration, JHEP **06** 2015 190
- [8] J. Adam et al., ALICE Collaboration, Phys. Rev. Lett. **116** (2016) 132302
- [9] G. Aad et al., ATLAS Collaboration, Phys. Lett. B **707** (2012) 330
- [10] G. Aad et al., ATLAS Collaboration, Phys. Rev. C **86** (2012) 014907
- [11] G. Aad et al., ATLAS Collaboration, JHEP **11** (2013) 183
- [12] S. Chatrchyan et al., CMS Collaboration, Eur. Phys. J. C **72** (2012) 2012
- [13] S. Chatrchyan et al., CMS Collaboration, Phys. Rev. C **87** (2013) 014902
- [14] S. Chatrchyan et al., CMS Collaboration, Phys. Rev. C **89** (2014) 044906
- [15] S. Chatrchyan et al., CMS Collaboration, JHEP **02** (2014) 088
- [16] V. Khachatryan et al., CMS Collaboration, Phys. Rev. C **92** (2015) 034911
- [17] A. M. Sirunyan et al., CMS Collaboration, Phys. Rev. C **96** (2017) 064902
- [18] B. Alver et al., PHOBOS Collaboration, Phys. Rev. Lett. **98** (2007) 242302
- [19] B. Alver et al., PHOBOS Collaboration, Phys. Rev. C **77** (2008) 014906
- [20] B. Alver and G. Roland, Phys. Rev. C **81** (2010) 054905
- [21] R. S. Bhalerao, M. Luzum and J.-Y. Ollitrault, Phys. Rev. C **84** (2011) 034910

- [22] E. Retinskaya, M. Luzum, and J.-Y. Ollitrault, *Phys. Rev. C* **89** (2014) 014902
- [23] G. Giacalone, J. Noronha-Hostler, and J.-Y. Ollitrault, *Phys. Rev. C* **95** (2017) 054910
- [24] J.-Y. Ollitrault, *Phys. Rev. D* **48** (1993) 1132
- [25] S. Voloshin, and Y. Zhang, *Z. Phys. C* **70** (1996) 665
- [26] N. Borghini, P. M. Dinh, and J.-Y. Ollitrault, *Phys. Rev. C* **63** (2011) 054906
- [27] N. Borghini, P. M. Dinh, and J.-Y. Ollitrault, *Phys. Rev. C* **64** (2001) 054901
- [28] A. Bilandzic, R. Snellings, and S. Voloshin, *Phys. Rev. C* **83** (2011) 044913
- [29] S. A. Voloshin, A. M. Poskanzer, A. Tang, and G. Wang, *Phys. Lett. B* (2008) **659** 537
- [30] A. M. Sirunyan et al., CMS Collaboration, *Phys. Lett. B* **789** (2019) 643
- [31] S. Acharya et al., ALICE Collaboration, *JHEP* **07** (2018) 103
- [32] L. Yan, J.-Y. Ollitrault, and A. M. Poskanzer, *Phys. Lett. B* **742** (2015) 290
- [33] G. Giacalone, L. Yan, J. Noronha-Hostler, and J.-Y. Ollitrault, *Phys. Rev. C* **95** (2017) 014913
- [34] CMS Collaboration, CMS-PAS-HIN-21-010, <https://cds.cern.ch/record/2806158>
- [35] A. M. Sirunyan et al., CMS Collaboration, *JINST* **15** (2020) P10017
- [36] V. Khachatryan et al., CMS Collaboration, *JINST* **12** (2017) P01020
- [37] S. Chatrchyan et al., CMS Collaboration, *JINST* **3** (2008) S08004
- [38] CMS Collaboration, CMS-PAS-LUM-18-001, <https://cds.cern.ch/record/2809613>
- [39] L. Nadderd, J. Milosevic, and F. Wang, *Phys. Rev. C* **104** (2021) 034906
- [40] R. S. Bhalerao, G. Giacalone, and J.-Y. Ollitrault, *Phys. Rev. C* **99** (2019) 014907